PAPER • **OPEN ACCESS**

Field calibration for multidirectional spectroradiometers

OPEN ACCESS
IOP Publishing
Measurement Science and Technology
Meas. Sci. Technol. **33** (2022) 065904 (9pp)
https://doi.org/10.1088/1361-6501/ac56be

Field calibration for multidirectional spectroradiometers

Angelika Niedzwiedz*, Jens Duffert, Mario Tobar-Foster, Jan Wilko Heinzel and Gunther Seckmeyer

Institut für Meteorologie und Klimatologie, Leibniz Universität Hannover, Herrenhäuser Str 2, D-30419 Hannover, Germany

E-mail: niedzwiedz@muk-uni-hannover.de

Received 13 August 2021, revised 17 January 2022
Accepted for publication 18 February 2022
Published 11 March 2022

Abstract

A mobile calibration system for a multidirectional spectroradiometer (MUDIS) to transfer the absolute radiometric calibration from the laboratory to the location of the outdoor-measurement (field calibrator) has been developed. The main part of the calibration system comprises an aluminium sphere with a diameter of 40 cm, mounting adapters and a ventilation system. The MUDIS device is capable of measuring spectral radiance from 320 to 600 nm in 113 different directions simultaneously within 1 s. When repeating radiance measurements inside the mobile field sphere, the relative standard deviation (RSD) for wavelengths between 320 and 600 nm is less than 1.8% (320 nm) for all directions with minimum RSD of 0.6% at 382 nm. The reproducibility depends not only on the wavelength but also on the individual fibre position on the hemispherical input optics, with maximum of 4.5% RSD, but most directions show a lower deviation. On average, the RSD for the channels is less than 0.9%. The calibrator enables measurements of the spectral radiance with less uncertainty than with the previous indirect calibration method, which uses measurements of a scanning reference array spectroradiometer.

Keywords: field calibration, multidirectional, multidirectional spectroradiometer (MUDIS), spectral radiance, reproducibility

(Some figures may appear in colour only in the online journal)

1. Introduction

Measurements of the sky radiance (see DIN 5031-1 1982) provide information on the interaction of solar radiation with atmospheric components, such as clouds, aerosols and trace gases (Dubovik and King 2000, Hönninger *et al* 2004, Feister and Shield 2005, Hirsch *et al* 2012) as well as their impact on the biosphere (Bao *et al* 2018, Schrempf *et al* 2017). Furthermore, they can also be used as input parameters for radiative transfer models (Thomas and Stamnes 1999, see Dubovik and King 2000, Igawa *et al* 2004, Hirsch *et al* 2012) or prediction models of solar systems (Gueymard and Ivanova 2018). The multidirectional spectroradiometer (MUDIS) (Riechelmann *et al* 2013, Riechelmann 2014), is capable of measuring radiance from 113 different directions (channels) simultaneously within milliseconds, so that rapid changes in the atmosphere (such as cloud movement) can be detected. To ensure the long-term stability and quality of the data, the device has to be calibrated at regular intervals (McKenzie *et al* 1997, Seckmeyer *et al* 2010, Bohn and Lohse 2017). For this purpose, two methods were presented for the MUDIS: an intercalibration with a scanning device under changing outdoor conditions (Riechelmann *et al* 2013, Riechelmann 2014) and an absolute calibration in the laboratory with an integrating sphere (Walker *et al* 1987, Niedzwiedz *et al* 2021). In the first case, there was no transfer method, either from the laboratory to field or back, to determine the

* Author to whom any correspondence should be addressed.

stability of the instrument and/or possible changes during transport, assembly and disassembly. Nevertheless, transfer methods for field calibrations during the outdoor campaigns are important parts of quality control for measurements of sky radiation (Gröbner *et al* 2005, Pissula *et al* 2009, Bohn and Lohse 2017, Zuber *et al* 2018). Some possible quality control methods include the use of absorption lines from the atmosphere or a monochromatic light source (e.g. pen lamps) (Dunagan *et al* 2013, Riechelmann 2014, Zuber *et al* 2018) Common methods of field calibrations are based on standard lamps. This type of traveling lamp is mounted in a protective housing against environmental influences (light, wind, etc) with an opening to attach the entrance optics (Seckmeyer 1989, Seckmeyer *et al* 1996, Early *et al* 1998, Harrison *et al* 2003, Bohn and Lohse 2017). Another regular method is the use of mobile integrating spheres (Brown and Johnson 2003) with a uniform inner coating of high reflective diffuse material with the working principle of an Ulbricht sphere (Walker *et al* 1987, Hanssen 2001, Butler *et al* 2003, Hanselaer *et al* 2009, Gigahertz-Optik 2020a, 2020b). For both methods, it is important to know the traceability to a primary standard with its uncertainties (Walker and Thompson 1994, Johnsen *et al* 1996, Bernhard and Seckmeyer 1999, Pissulla *et al* 2009) and to ensure an accurate and high-precision power supplies. It should be noted that integrating spheres depend on the type of construction and the reflective material (powder or solid). Powdery material can flake off during assembly and disassembly and is sensitive to humidity. This can lead to large variations of the surface that may be interpreted as unavoidable uncertainties in the performance of the measuring device. In the case of field calibration method based on standard lamps inside of a housing, it has to be taken into account that the emission of lamps may be influenced by weather conditions (e.g. wind, sunlight) and the varying outdoor temperature, which may increase the uncertainties of the calibration. With both methods, it is possible to calibrate only one direction of the input optics at a one time, which proved to be quite time-consuming for multidirectional devices.

For the transfer of the spectral radiance calibration for outdoor measurements of multidirectional optics, the following requirements have been identified:

(a) All channels (directions) shall be illuminated simultaneously. This is a great advantage, because the time for the calibration process is considerably reduced compared to the previously described methods.
(b) The input optics, which consists of fibres with different directions, must not be moved between calibration and measurement of solar radiance because changes of the spectral responsivity due to bending of the fibres need to be avoided (Riechelmann 2014).
(c) The system has to be protected against weather influences and solar radiation, to ensure the stability of the lamp emission and to avoid unwanted exposure to sunlight. The current and voltage needs to be monitored and its stability needs to be ensured by high-precision power supply units.
(d) The system needs to be designed robust for mobile and frequent use and suitable for all ground structures.
(e) Reproducibility is the primary goal of the device, because it is transfer standard only, inhomogenities of spectral radiance inside the sphere are not important. The traceability to a primary standard is described in Niedzwiedz *et al* (2021).

2. Materials and methods

2.1. Multidirectional spectroradiometer (MUDIS)

MUDIS is a multidirectional spectroradiometer that measures spectral sky radiance simultaneously in a wavelength range of 250–600 nm (only 300–550 nm should be used if a reasonable uncertainty needs to be achieved). It consists of 113 optical fibres (figures 1 and 2) mounted in a hemispherical dome (figure 1), an Offner spectrometer (3) and a UV sensitive CCD camera (4). The fibres, which are aligned in different directions on the dome, and bundled together (2), are lined up in a row and inserted into the spectrometer. The recorded images contain information about the direction and spectral range of the detected sky radiance, the time and the radiance. For further details, see (Riechelmann *et al* 2013, Riechelmann 2014).

2.2. Integrating spheres

An aluminium sphere with a diameter of 40 cm was constructed for the field calibration (UK40), which is large enough to host the MUDIS hemispherical dome.

2.2.1. Measurement setup. The sphere for field calibration has a diameter of 40 cm and is made of aluminium. In contrast to many other Ulbricht spheres, which have a high reflective coating or material inside (Walker *et al* 1987), the inner wall of the UK40 was sandblasted to create a diffuse surface (figure 2(a)), but no special emphasis has been given to high reflectance. Inside the sphere, there are three 100 Watt halogen lamps, which are fixed 120° to each other. The radiation from the lamps is reflected randomly several times by the sandblasted inner surface, creating a diffuse radiation field as in the case of an Ulbricht sphere with high reflectance (see Walter *et al* 1987) but the spectral radiance is not homogeneous. At the opening of the sphere, a small deepening is located (figure 2(a), black area), which in combination with a retaining ring and the corresponding triangular pin on it (figure 3) ensures the reproducibility of the setup. Eventually a ventilation unit is installed over the UK40 to dissipate the heat produced by the three 100 Watt lamps to prevent possible heat damage and solar radiation from the outside (figure 3, left).

After the absolute calibration with a bigger Ulbricht sphere (UK100) (Niedzwiedz *et al* 2021) the retaining ring with the triangular pin (figure 3, top right) is fixed directly under the unmoved input optics dome (white weather protection) using three ring holders (figures 2(c) and 3, middle). In 2nd step the

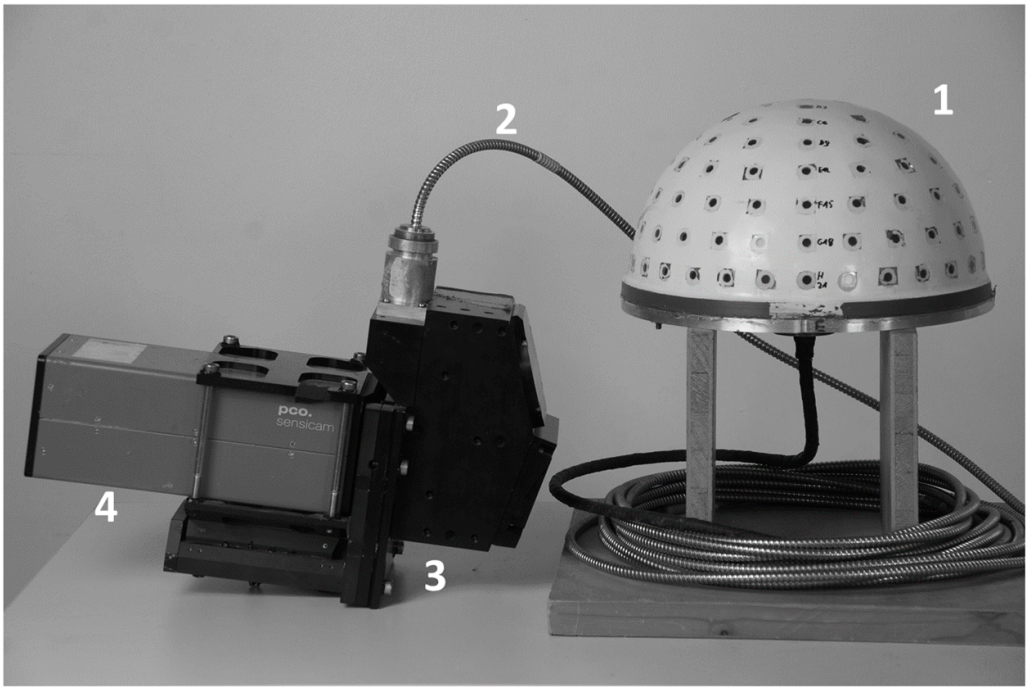

Figure 1. Picture of the MUDIS shows the entrance optics dome (1) with weather protection (white), the fibre bundle (2) with the 113 different directions fixed into the dome, the Offner imaging spectrometer (3) and the UV-sensitive CCD camera (4). Reproduced with permission from Schilke (2020).

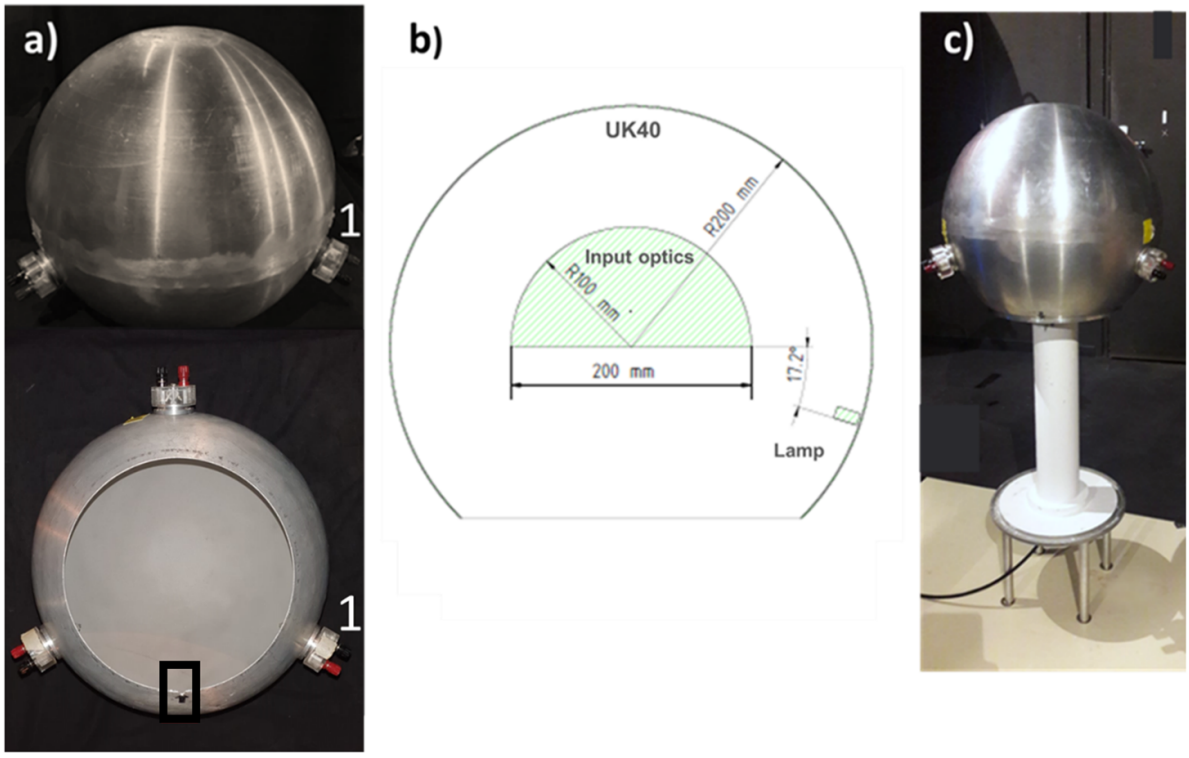

Figure 2. (a) Top: transfer calibration integration sphere with the power connectors for three 100 Watt lamps (1). Bottom: the sandblasted inner surface of the aluminium sphere with the power connectors for three 100 Watt lamps (1). Black area: deepening for the pin of the retaining ring for the reproducible holding of the UK40. (b) Technical sketch and adjustment concept of a multidirectional entrance optics inside the UK40. The lamps are located in the lower hemisphere so that no direct light should reach the fibres. Reproduced with permission from Tobar-Foster (2021). (c) Measurement setup for transfer calibration in the laboratory after absolute calibration of the MUDIS. The UK40 is mounted on a specially designed mounting ring (figure 3) with a corresponding pin of the UK40 (black area, picture (a)). The MUDIS optical dome is located inside the UK40 and fixed to the barium sulphate socket without any moving between the absolute calibration and the transfer calibration.

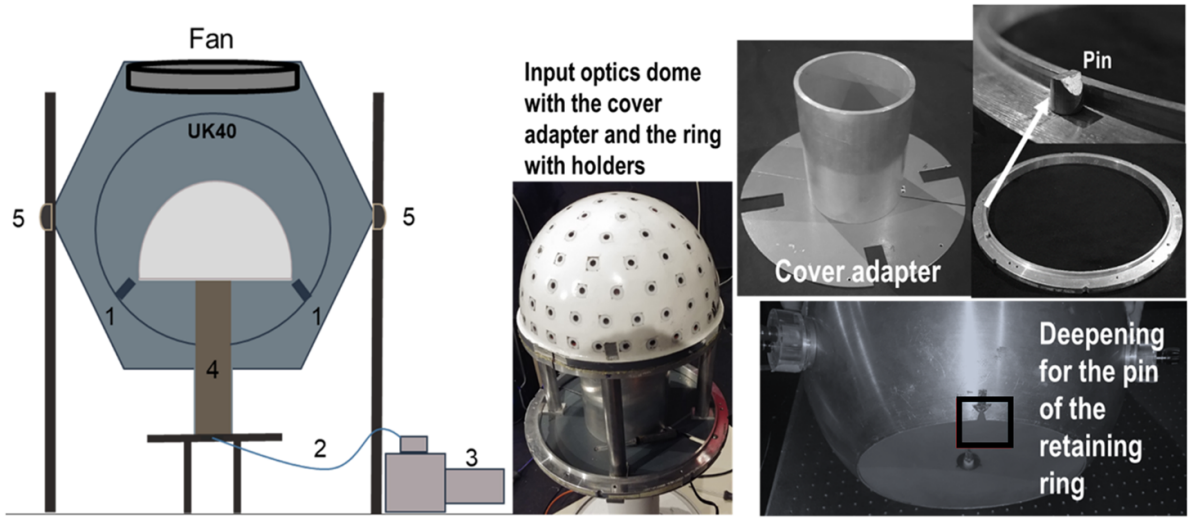

Figure 3. Left: sketch of the measurement setup of the UK40 inside the shading and ventilation system (dark grey container). The ventilation system consists of an industrial fan built into a plastic container and adjustable aluminium tubes as holders (5). For reasons of legibility, the retaining ring for the UK40 has not been included in the drawing. (1) 100 Watt lamps, (2) fibre bundle, (3) spectrometer and CCD camera system, (4) in the laboratory: barium sulphate socket with the fixed MUDIS optic on it. Middle: the input optics dome with the fixed retaining ring on the tree holders attached to the white weather protection. Mounted to the ring is the cover adapter, which encloses the barium sulphate socket. Top right: components of the system like the cover adapter and the holder ring with the triangular pin for the UK40. Bottom: deepening for the pin (triangular shape) of the retaining ring at the opening of the UK40.

cover adapter (figure 3, top right) is mounted on the retaining ring in order to enable comparability of the measurements of the radiation field within the UK40 and to exclude further light influence from outside. The adapter avoids further uncertainties caused by differently reflecting materials within the UK40, e.g. the white barium sulphate socket (figure 2(c)) in the laboratory would otherwise generate a different radiation field within the UK40 than the grey aluminium tube on the measuring platform, with the result that the relative calibration would no longer be transferable. Both mentioned tubes are used as holders for the optical dome. In the 3rd step, the UK40 is mounted on the pin (triangular shape) of the ring with the corresponding deepening (figure 3, bottom) at the opening of the sphere until it is locked in place, so that no movement of the UK40 on the ring is possible and the reproducibility of the installation is ensured. The UK40 is mounted on the holder ring and the three lamps (figure 2) inside the sphere are then below the horizon of the input optics. Therefore, no direct radiation from the lamps should reach the fibres within their field of view (FOV). For operation, the ventilation system is mounted over the UK40 (figure 3, left). In the fourth and final step of the transfer calibration, the complete system (measuring instrument and calibration equipment) is set up at the location of the measurement campaign and further measurements with the UK40 are carried out for the comparison and verification of the calibration chain.

3. Reproducibility

Since the UK40 is used to transfer the calibration from the laboratory to field (outdoor) measurement the reproducibility of the setup has been investigated.

3.1. Measurement setup

The UK40 was repeatedly mounted and dismounted from the holding ring with the pin and the ventilation system. The temperature and voltage were logged. A measurement was only started when temperature inside the sphere (zenithal area) was stable within ± 0.5 K and the lamp current was stable within ± 0.001 A. A series of six measurements was carried out for the investigation, which were compared to each other.

3.2. Results

In this study of the reproducibility, the 1st measurement (sample 1) was compared with the following measurements (ratio of sample 2, 3…/sample 1). Figure 7 shows an example of the ratio between the first (sample 1) and the last measurement (sample 6) for all directions in the wavelength range 320–600 nm. Four fibres (4, 52–54), which had too low or too high signal, are not shown in the graphs, but were included in the calculation.

It can be recognized from the graph (figure 4) that the reproducibility below 350 nm (sensor range area) fluctuates up to 10% for some directions due to the low spectral radiance in this wavelength range; above 360 nm the deviation is less than 5% in all directions. Furthermore, it can also be seen that the deviation depends on the direction of the fibre. The comparison of the other five measurements has shown a similar behaviour. The maximum deviation in these ratios is up to 21.2% for fibre 4 (not in the figure 4). The high deviation at this position is due to the fact that it is one of the fibres with a very low sensitivity.

The reproducibility for all 113 channels was further analysed by comparing individual measurements to the mean

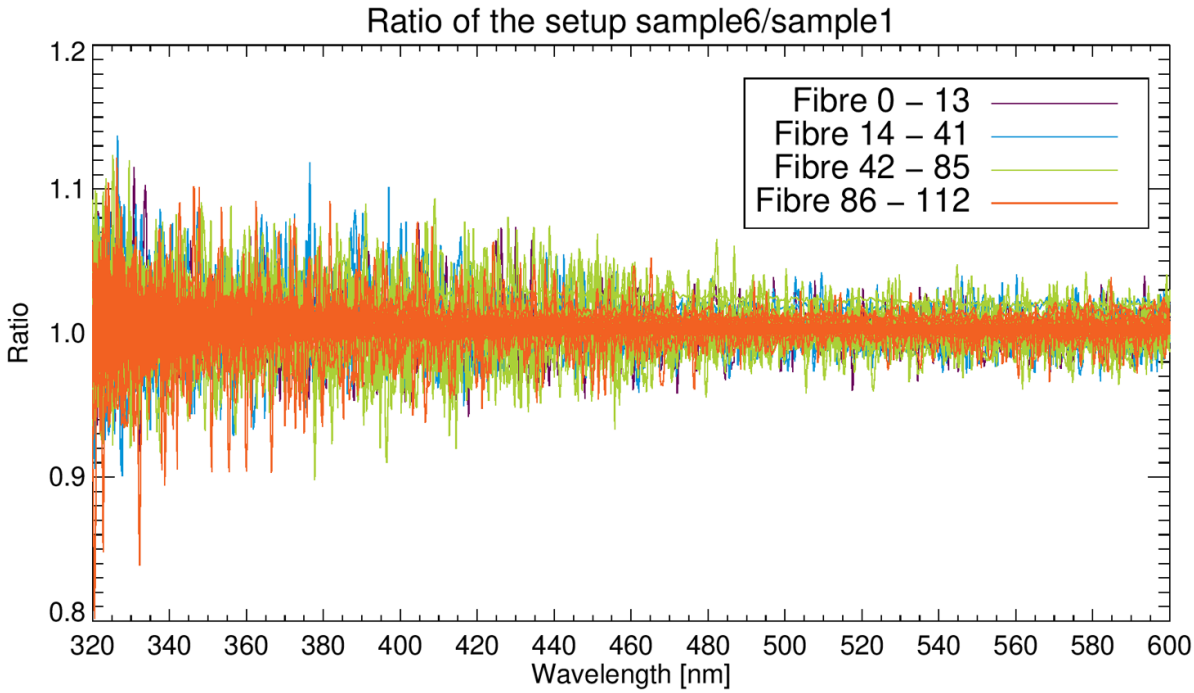

Figure 4. The example of the ratio (ordinate) between the first (sample 1) and the last measurement (sample 6) for all directions in the wavelength range 320–600 nm (abscissa). Since more than 100 directions are shown, the positions of the fibres on the input optics were divided into sectors from zenithal areas (0–13) to horizontal areas (86–112). Four fibres (4, 52–54) with a too low or too high signal were removed in the graph but taken into account in the subsequent calculation. On average, the ratio fluctuates by 1% and shows a good reproducibility.

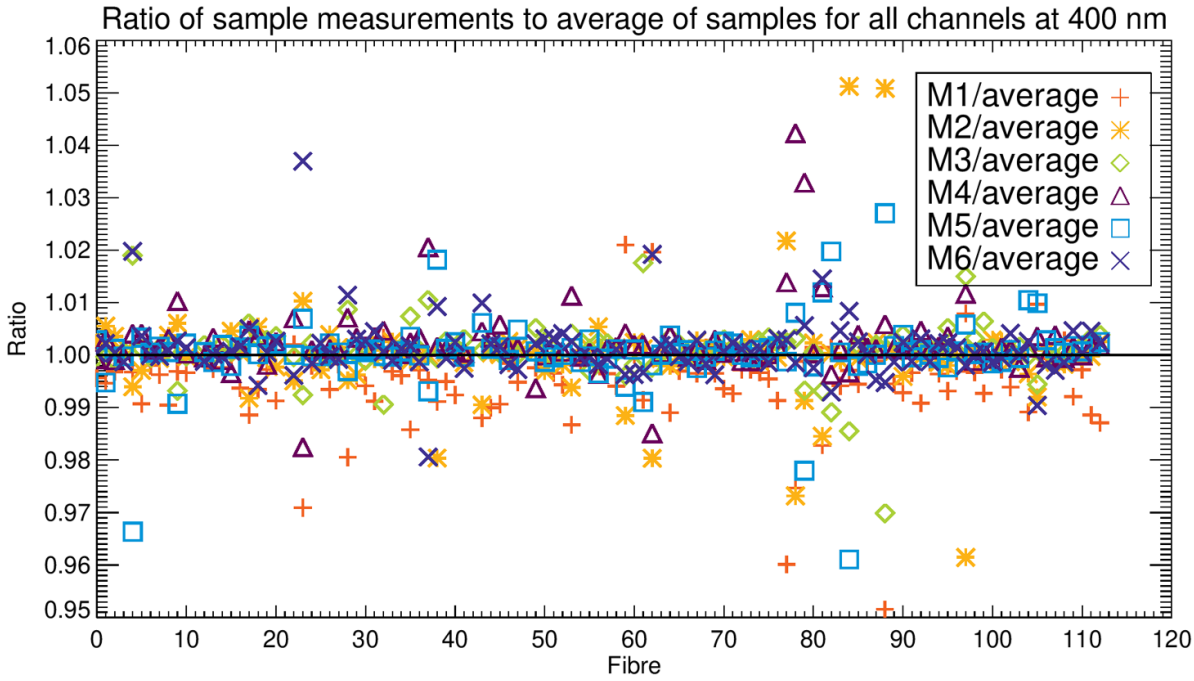

Figure 5. Ratio of sample measurements to average of samples for all channels (fibre positions) at 400 nm. The abscissa represents the position of the fibres from zenith (0) to the horizon (112). The measurements show a satisfactory reproducibility of the field calibration measurements for nearly all directions.

value of all sample measurements of each direction for specific wavelengths.

The abscissa in the figure 5 represents the position of the fibres from zenith (fibre 0) to the horizon (fibre 112). The ordinate the ratio of the sample measurement to the average of all samples at 400 nm. However, all deviations are smaller than 5%. The deviations for directions 0–75 are less than 2.4% on average, the highest deviation occurred in sample M6

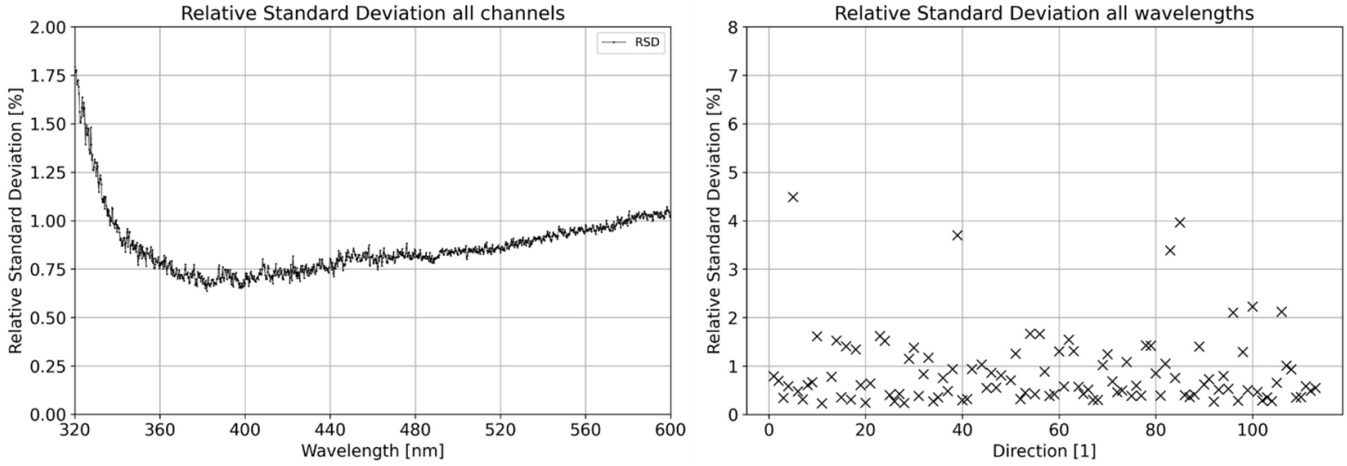

Figure 6. The RSD was calculated from all sample measurements according to equation (1) over all channels (left) and wavelengths (right). Left: the abscissa represents the wavelength in the range of 320–600 nm, the ordinate the variation of the RSD of all measurements. Right: the abscissa represents the position of the fibres from zenith (0) to the horizon (112), the ordinate the variation of RSD of all measurements. Reproduced with permission from Tobar-Foster (2022).

(M6/average) with 3.6%. Fibres with larger deviations have received either too little or too much signal. In general, the measurements show a satisfactory reproducibility of the field calibration measurements for nearly all directions.

Finally, the relative standard deviation (RSD, equation (1)) was calculated for the reproducibility measurement of all samples (M_i, $i = 1-6$) for the wavelengths and direction (channel) with the ratio of standard deviation ($\mathrm{SD}^{\mathrm{wave}}_{\mathrm{channel}}$) to the mean ($\mathrm{Mean}^{\mathrm{wave}}_{\mathrm{channel}}$).

$$\mathrm{RSD}^{\mathrm{wave}}_{\mathrm{channel}} = \left(\sum_i \frac{\mathrm{SD}^{\mathrm{wave}}_{\mathrm{channel}}}{\mathrm{Mean}^{\mathrm{wave}}_{\mathrm{channel}}} \times M_i \right) \times 100, \quad \text{with } i = 1-6, \text{ in } [\%]. \tag{1}$$

In figure 6 both graphs illustrates the RSD over all sample measurements according to equation (1) for all channels (left) and wavelengths (right). In the left graph (figure 6, left) the maximum of the RSD is less than 1.8% at 320 nm. The minimum amounts 0.6% at 382 nm. For the directional dependence calculation of the RSD (figure 6, right), the maximum RSD results at fibre 4 (four starting from zero) with 4.5% and the minimum RSD is at fibre 10 with 0.2%. On average for all directions over all samples, the RSD is less than 0.9%. In addition, the RSD of individual fibres exceed 4.2% RSD can be recognized in this graph (figure 6, right). The higher deviations of the individual fibres may be due to irregularities caused by the sandblasting, which then leads to oversaturation (e.g. direct reflection) or too low signals.

Summarizing, a wavelength and direction dependent reproducibility is observed due to the FOV wavelength dependence of the fibres (Riechelmann 2014), the spectral sensitivity of the sensor (Riechelmann 2014), the geometry of the measurement setup (smaller area for multiple reflections) as well as of martial properties (sandblasted aluminium surface). Nevertheless, the values determined are sufficient enough in the context of the relative method for a transfer measurement between the laboratory and the measurement field.

4. Radiance distribution within the sphere UK40

4.1. Measurement setup

For the determination of the radiance distribution within the UK40, the sphere with adapters, ring and ventilation system (according to section 2.2.1, figure 3) was attached to the pre-calibrated MUDIS (Niedzwiedz *et al* 2021), directly after the absolute calibration and without movement.

In the 1st step, the spectral sensitivity ($S_{\mathrm{MUDIS}}(\lambda)$) of the pre-calibrated MUDIS for every direction is determined by:

$$S_{\mathrm{MUDIS}}(\lambda) = \frac{M_{\mathrm{UK100}}(\lambda)}{L_{\mathrm{Zenith}}(\lambda)} \tag{2}$$

where $M_{\mathrm{UK100}}(\lambda)$ is the measured spectral signal detected in the calibration sphere (Ulbrichtkugel of 100 cm diameter (UK100, measured in unit Counts) (Niedzwiedz *et al* 2021). $L_{\mathrm{Zenith}}(\lambda)$ is the zenith radiance of the UK100, which was determined by a pre-calibrated scanning instrument, the mobile reference spectroradiometer of the network for the detection of atmospheric composition change (NDACC) (Wuttke *et al* 2006, Pissula *et al* 2009, Niedzwiedz *et al* 2021). $S_{\mathrm{MUDIS}}(\lambda)$ has the unit $[S] = \left[\frac{M}{L}\right] = \frac{\mathrm{Counts}}{\mathrm{W\,m^{-2}nmsr}}$.

In step 2, without moving the input optic and the optical fibre, the UK40 (according to section 2.2.1, figure 3) was placed centrally on the entrance dome, so that the spectral radiance of all fibres inside the sphere ($L_{\mathrm{UK40}}(\lambda)$) was detected by using the pre-calibrated MUDIS ($M_{\mathrm{UK40}}(\lambda)$) and calculated with the spectral sensitivity ($S_{\mathrm{MUDIS}}(\lambda)$) to:

$$L_{\mathrm{UK40}}(\lambda) = \frac{M_{\mathrm{UK40}}(\lambda)}{S_{\mathrm{MUDIS}}(\lambda)}. \tag{3}$$

A description and list of the components and uncertainties of the pre-calibrated NDACC instrument and the calibration of MUDIS within the UK100 is given in Niedzwiedz *et al* (2021) (sections 4 and 5). The NDACC instrument was calibrated according to Pissulla *et al* (2009).

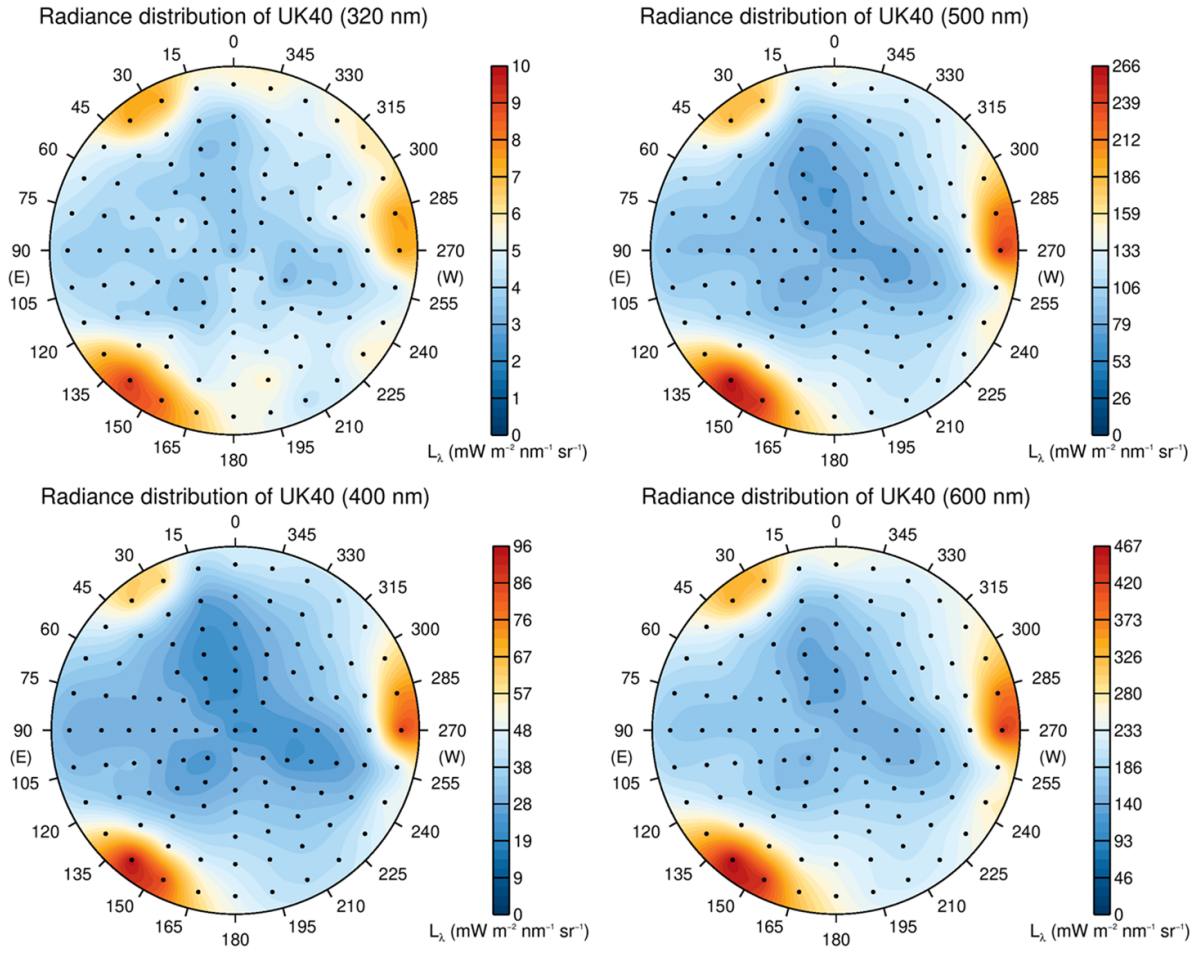

Figure 7. Radiance distribution inside the UK40 at wavelength 320 nm, 400 nm, 500 nm and 600 nm visualized in a polar plot. The black dots represent the fibres positions. The impact area of the lamps or a direct reflection at the surface of the sphere may be recognized in the high values orange coloured areas.

4.2. Results

Figure 7 shows polar contour plots of the spectral radiance distribution of the hemisphere inside the UK40 in dependence of the zenith and azimuth directions for the wavelength 320 nm, 400 nm, 500 nm and 600 nm. The black dots represent the 113 fibres positions interpolated with the Kriging interpolation method (Isaaks and Srivastava 1989).

In figure 7 the geometrical position of the lamps can be recognized at all wavelengths. Furthermore, it can be seen that radiance distribution is not homogeneous. However, this finding is not surprising and it is a consequence of the small diameter of the sphere and of the optical properties of the inner surface of the sphere. The spectral radiance at 320 nm is lower than at higher wavelengths because of a lower spectral emission of the lamps in this range (low signal-to-noise ratio) and due to higher absorption of UV of the aluminium surface. It should be noted that a homogenous radiance field is not required for a transfer source. It has never been intended to construct an absolute field calibrator, just a relative transfer. Therefore only reproducibility must be ensured.

5. Discussion and conclusion

The central intention of this article was to present a concept for a mobile calibration transfer device. It is a relative calibration for a MUDIS and enable the transfer of calibration from the laboratory to outdoor measurements. The presented system consists of an aluminium sphere with a diameter of 40 cm, whose inner surface has been sandblasted and illuminated with 3 $\times$ 100 Watt lamps. Uncertainties of the construction of this concept compared to the classical properties of an integrating sphere (Walker *et al* 1987) were taken into account and their influence was investigated. The uncertainty due to voltage/current changes (Walker and Thompson 1994, Bernhard and Seckmeyer 1999) can be neglected as the lamps are operated with accurate power supplies, which operate the lamps at 8 ± 0.001 A. The aging of the reference standards and burning time of the lamps, which affect the emission characteristics, (Bernhard and Seckmeyer 1999) have been less than 30 h for the absolute calibration of the MUDIS (section 4). Two further properties of the setup, which have to be kept in mind, are the absorption properties of the aluminium and the structure of the grain size of the sandblasted inner surface of

the sphere. Furthermore, the significant reduction of the output signal, especially in the signal low UV range, can be explained by the multiple reflections inside the sphere. Since the absorption depends on the wavelength and increases with decreasing wavelengths (Haferkorn 2003), this effect is probably multiplied especially for the upper sphere. However, this characteristic has a significant influence on the signal intensity but no direct impact on the relative calibration method, as long as the setup is reproducible enough.

To determine the inhomogeneity of the sandblasted inner surface of the UK40, the surface was first analysed under a microscope. The differences in grain size varied from 10 µm to 200 µm, which means that the reflections within the sphere cannot be uniformly distributed. The radiance field distribution is therefore not only dependent on the FOV of the fibre, but also on the viewing point to the surface. Therefore, it is even more important to have a reproducible setup. The spectral radiance inside the sphere is not homogeneous as shown in figure 6 (section 4). Despite higher inhomogeneities in the radiance field of the UK40, which occur only for a few directions reproducible measurements can be achieved with 1% on average. When analysing all directions a RSD from 0.2% to 1.8% has been found between 320 and 600 nm. This leads to the conclusion that the UK40 system can be used to detect sensitivity changes of the MUDIS, which may occur by transport of the equipment between the laboratory and the location of outdoor measurements.

Data availability statement

The data that support the findings of this study are available upon reasonable request from the authors.

Acknowledgments

We thank Holger Schilke and Ulrich Meyer for technical support. As well as Lars Schneider for his support during the planning phase and Stefan Riechelmann for his support during the planning phase and analysis.

ORCID iD

Angelika Niedzwiedz https://orcid.org/0000-0002-2115-379X

References

Bao T, Zhu R, Wang P, Ye W, Ma D and Xu H 2018 Potential effects of ultraviolet radiation reduction on tundra nitrous oxide and methane fluxes in maritime Antarctica *Sci. Rep.* **8** 3716

Bernhard G and Seckmeyer G 1999 Uncertainty of measurements of spectral solar UV irradiance *J. Geophys. Res. Atmos.* **104** 14321–45

Bohn B and Lohse I 2017 Calibration and evaluation of CCD spectroradiometers for ground-based and airborne measurements of spectral actinic flux densities *Atmos. Meas. Tech.* **10** 3151–74

Brown S and Johnson B 2003 Development of a portable integrating sphere source for the Earth Observing System's calibration validation program *Int. J. Remote Sens.* **24** 215–24

Butler J J, Brown S W, Saunders R D, Johnson B C, Biggar S F, Zalewski E F, Markham B L, Gracey P N, Young J B and Barnes R A 2003 Radiometric measurement comparison on the integrating sphere source used to calibrate the moderate resolution imaging spectroradiometer (MODIS) and the Landsat 7 enhanced thematic mapper plus (ETM+) *J. Res. Natl Inst. Stand. Technol.* **108** 199–228

DIN 5031 Teil 1 1982 *Strahlungsphysik im optischen Bereich und Lichttechnik* (Berlin: Beuth)

Dubovik O and King M D 2000 A flexible inversion algorithm for retrieval of aerosol optical properties from sun and sky radiance measurements *J. Geophys. Res. Atmos.* **105** 20673–96

Dunagan S E, Johnson R, Zavaleta J, Russell P B, Schmid B, Flynn C, Redemann J, Shinozuka Y, Livingston J and Segal-Rosenhaimer M 2013 Spectrometer for sky-scanning sun-tracking atmospheric research (4STAR): instrument technology *Remote Sens.* **5** 3872–95

Early E, Thompson E and Disterhoft P 1998 Field calibration unit for ultraviolet spectroradiometers *Appl. Opt.* **37** 6664–70

Feister U and Shields J 2005 Cloud and radiance measurements with the VIS/NIR daylight whole sky imager at Lindenberg (Germany) *Meteorol. Z.* **14** 627–39

Gigahertz-Optik 2020a Gigahertz-Optik GmbH Türkenfeld (available at: www.gigahertz-optik.de/de-de/produkt/UPK-50-L, www.gigahertz-optik.de/de-de/service-und-support/informationsportal/odm-material/, www.gigahertz-optik.de/de-de/service-und support/informationsportal/grundlagen-lichtmesstechnik/ulbrichtkugeln/ideale-ulbrichtkugel/) (Accessed 20 May 2020)

Gigahertz-Optik 2020b Gigahertz-Optik GmbH Türkenfeld (available at: www.gigahertz-optik.de/de-de/produkt/UMTB-1000, www.gigahertz-optik.de/de-de/produkt/ODP97) (Accessed 4 December 2020)

Gröbner J *et al* 2005 Traveling reference spectroradiometer for routine quality assurance of spectral solar ultraviolet irradiance measurements *Appl. Opt.* **44** 5321–31

Gueymard C and Ivanova S 2018 Progress in Sky Radiance and Luminance Modeling Using Circumsolar Radiation and Sky View Factors *EuroSun 2018* (*Rapperswil, Switzerland*) (https://doi.org/10.18086/eurosun2018.09.16)

Haferkorn H 2003 *Optik Physikalisch-technische Grundlagen und Anwendungen* 4. Auflage (Weinheim: Wiley)

Hanselaer P, Keppens A, Forment S, Ryckaert W R and Deconinck G 2009 A new integrating sphere design for spectral radiant flux determination of light-emitting diodes *Meas. Sci. Technol.* **20** 095111

Hanssen L 2001 Integrating-sphere system and method for absolute measurement of transmittance, reflectance, and absorbance of specular samples *Appl. Opt.* **40** 3196–204

Harrison L, Beauharnois M, Berndt J, Kiedron P and Disterhoft P 2003 Transfer of UV irradiance calibration to our field spectroradiometers: current performance and operational experience at table Mt. CO *Proc. SPIE* **5156** 135–42

Hirsch E, Agassi E and Koren I 2012 Determination of optical and microphysical properties of thin warm clouds using ground based hyper-spectral analysis *Atmos. Meas. Tech.* **5** 851–71

Hönninger G, von Friedeburg C and Platt U 2004 Multi axis differential optical absorption spectroscopy (MAX-DOAS) *Atmos. Chem. Phys.* **4** 231–54

Igawa N, Koga Y, Matsuzawa T and Nakamura H 2004 Models of sky radiance distribution and sky luminance distribution *Sol. Energy* **77** 137–57

Isaak E H and Srivastava R M 1989 *An Introduction to Applied Geostatistics* (NY: Oxford University Press)

Johnson C, Bruce S, Early E, Houston J, O'Brian T, Thompson A, Hooker S and Mueller J 1996 The fourth seawifs intercalibration round-robin experiment (sirrex-4) *Technisches Memorandum* vol 37 (Greenbelt, MD: NASA Goddard Space Flight Center)

McKenzie R L, Johnston P V and Seckmeyer G 1997 UV spectro-radiometry in the network for the detection of stratospheric change (NDACC) *Solar Ultraviolet Radiation. Modelling, Measurements and Effects* (Berlin: Springer) pp 279–87

Niedzwiedz A, Duffert J, Tobar-Foster M, Quadflieg E and Seckmeyer G 2021 Laboratory calibration for multidirectional spectroradiometers *Meas. Sci. Technol.* **32** 095902

Pissulla D *et al* 2009 Comparison of atmospheric spectral radiance measurements from five independently calibrated systems *Photochem. Photobiol. Sci.* **8** 516–27

Riechelmann S 2014 Simultaneous measurement of spectral sky radiance: development, characterization and validation of a non-scanning multidirectional spectroradiometer (MUDIS) *Dissertation* Institut für Meteorologie und Klimatologie, Gottfried Wilhelm Leibniz Universität Hannover (https://doi.org/10.1039/c3pp50221j)

Riechelmann S, Schrempf M and Seckmeyer G 2013 Simultaneous measurement of spectral sky radiance by a non-scanning multidirectional spectroradiometer (MUDIS) *Meas. Sci. Technol.* **24** 125501

Schilke H 2020 Image source: figure 1: picture of the MUDIS The permission is available. Leibniz Universität Hannover, Institut für Meteorologie und Klimatologie. Herrenhäuser Str.2, 30419 Hannover

Schrempf M, Thuns N, Lange K and Seckmeyer G 2017 Einfluss der Verschattung auf die Vitamin-D-gewichtete UV-Exposition eines Menschen *Akt Dermatol.* **44** 204–9

Seckmeyer G 1989 Spektralradiometer für die Ökologische Pflanzenforschung *Licht* **41** 7–8

Seckmeyer G, Bais A, Bernhard G, Blumthaler M, Drueke S, Kiedron P, Lantz K, McKenzie R and Riechelmann S 2010 Instruments to measure solar ultraviolet radiation Part 4: Array spectroradiometers WMO TD No. 1538

Seckmeyer G, Bernhard G, Mayer B and Erb R 1996 High accuracy spectroradiometry of solar UV radiation *Metrologia* **32** 697–700

Thomas G and Stamnes K 1999 *Radiative Transfer in the Atmosphere and Ocean* (New York: Cambridge University Press)

Tobar-Foster M 2021 Figure source: figure 2(b): technical sketch input optics Leibniz Universität Hannover, Institut für Meteorologie und Klimatologie. Herrenhäuser Str.2, 30419 Hannover

Tobar-Foster M 2022 Figure source: figure 6: the relative standard deviation (RSD) Leibniz Universität Hannover Institut für Meteorologie und Klimatologie, 30419 Hannover

Walker J H and Thompson A 1994 Improved automated current control for standard lamps *J. Res. Natl Inst. Stand. Technol.* **99** 255

Walker J, Saunders R, Jackson J and McSparron D 1987 NBS measurement services: spectral irradiance calibrations *National Bureau of Standards Special Publication* (Center of Radiation Research, National Measurement Laboratory, National Bureau of Standards, US Department of Commerce) p 250

Wuttke S, Seckmeyer G, Bernhard G, Ehramjian J, McKenzie R, Johnston P and O'Neill M 2006 New spectroradiometers complying with the NDSC standards *J. Atmos. Ocean. Technol.* **23** 241–51

Zuber R, Ribnitzky M, Tobar M, Lange K, Kutscher D, Schrempf M, Niedzwiedz A and Seckmeyer G 2018 Global spectral irradiance array spectroradiometer validation according to WMO *Meas. Sci. Technol.* **29** 105801